Cohesive energies of Fe-based glass-forming alloys

M. Mihalkovic,* M. Widom, and L. Xie
Department of Physics
Carnegie Mellon University
(Dated: October 2, 2003)

We calculate the enthalpies of mixing of Fe-based glass-forming alloys in the B-Fe-Y-Zr quaternary system. Our *ab-initio* calculations fully relax atomic positions and lattice parameters. We examine both the known equilibrium and metastable phases of this alloy system as well as a selection of plausible structures drawn from related alloy systems. This method, which can be applied very generally to any alloy system, generally reproduces experimentally determined phase diagrams while providing additional information about energetics of metastable and unstable structures. In particular we can identify crystalline structures whose formation competes with the metallic glass. In some cases we identify previously unknown structures or observe possible experimental errors in the accepted phase diagrams.

PACS numbers: Valid PACS appear here

I. INTRODUCTION

The ability to calculate alloy phase diagrams from first-principles is essential if we are to achieve the goal of materials by design [1]. A useful test case for this approach is the study of bulk metallic glass-forming alloys, which often contain three or more chemical elements. Recently discovered many-component alloys[2–4] solidfy in amorphous structures at relatively low cooling rates, forming bulk samples of metallic glass. These materials display intriguing and potentially useful mechanical properties including nearly perfect elasticity[5]. Amorphous Fe-based alloys are of interest for both their structural and their magnetic properties, and achieving bulk glass formation could extend the range of potential applications of these materials. This is just one example where the ability to calculate phase diagrams from first principles is useful scientifically and technologically. Indeed, our methods could be used in the study of compounds used for permanent magnets [6]

To understand factors limiting bulk glass formation, we perform *ab-initio* total energy calculations on the quaternary compound B-Fe-Y-Zr as well as its binary and ternary subsystems such as B-Fe and B-Fe-Zr. Our calculations use the plane-wave electronic density functional theory program VASP [7, 8]. We focus on identifying the crystalline structures whose formation competes with the amorphous structure of the supercooled liquid. To this end, we calculate the cohesive energies of stable, metastable and hypothetical crystal structures throughout the alloy composition spaces. Known stable and metastable structures are taken from standard metallurgical databases [9–11]. Hypothetical structures are drawn from the known structures of chemically similar alloy systems.

Cohesive energies of stable and metastable phases yield thermodynamic driving forces for crystalization. The structural complexity of these phases gives some insight into the possibility of their nucleation and growth during a rapid quench. Our main results are the identification of the structure types Fe_3C (Pearson symbol oP16) and $Cr_{23}C_6$ (Pearson symbol cF116) as the two main competitors to the Fe-B glass. Alloying with Zr does surprisingly little to destabilize the $Cr_{23}C_6$ structure, while alloying instead with Y does reduce stability of this structure. On the other hand, alloying with Y stabilizes certain other ternary structures. On this basis we deduce limits on the most advantageous composition ranges.

Energetically favorable structural motifs identified within these phases can be compared with structural models of the metallic glass. We identify a class of Boron coordination polyhedra related to the trigonal prism [12] with some distortions. These polyhedra may be arranged in many ways, some leading to simple crystal structures with very low energy but many more whose energies and local structure closely resemble the glass. We call the entire class of these structures "amorphous approximants", by analogy with the concept of approximants to quasicrystal structures [13].

The following two sections of this paper (sections II and III) present our calculational methods and the resulting cohesive energy data. Although we study here Fe-based glass-forming alloy systems, our basic method can be applied to any alloy system. Although we largely reproduce the known experimental phase diagrams, our calculations provide energetic information which is often not known experimentally, especially in the case of metastable and amorphous structures. In addition, we are able to propose likely structures for several compounds whose existence was known but whose structures were unknown, specifically B_4Fe_4Y, B_4FeY and $B_6Fe_2Y_5$. Conversely, in some cases our results call into question details of the established phase diagrams. For example: the claimed high temperature stability of BZr is most likely only metastability in reality; the Fe_5Y structure, believed metastable, may well be truly stable at low temperatures;

*Also at Slovakian address

the phase $Fe_{17}Y_2$, potentially important as a permanent magnet material [6], is possibly only a high temperature phase. Further, we can predict phase diagrams of alloy systems such as BYZr and FeYZr that have not been established experimentally.

Finally, section IV analyzes the crystal structures and correlates their atomic arrangements with their cohesive energies. Amorphous approximants are presented in subsection IV C.

II. METHODS

The structures we investigate include binary B-Fe and ternary B-Fe-Zr and B-Fe-Y compound, which in turn lead to the study of all elemental, binary, ternary and quatenary combinations of the elements B-Fe-Zr-Y. We selected structures for study that are known as stable or metastable structures in the phase diagrams of these alloy systems or chemically similar alloy systems. For example we consider known C-Fe structures (e.g. CFe_3.oP16) with B replacing C, etc. Our notation for structure type is to first give the *prototype* (some familiar isostructural compound, e.g. CFe_3) followed by the *Pearson symbol* (indicating the point symmetry, centering information, and number of atomic sites per unit cell, e.g. oP16 for primitive orthorhombic 16-atom cell).

Our sources for established phase diagrams and structures are standard references [9–11]. Information from these sources has been compiled into a database containing over 800 structures that we search to match criteria such as chemical elements, stoichiometry, and atomic size ratios. Some additional structures examined are liquid and amorphous structures, obtained from *ab-initio* molecular dynamics simulation as discussed below in section IV B.

Our *ab-initio* calculations use the program VASP (version 4.5.5) together with the projector-augmented wave method, an all-electron generalization of the pseudopotential approach [14, 15]. We employ the Perdew-Wang generalized gradient approximation [16] (GGA) exchange-correlation functional with the Vosko-Wilkes Nussair [17] spin interpolation. These choices are known to give excellent results for bulk elemental Fe [15]. In particular, the use of GGA instead of LDA is necessary to properly reproduce magnetization and lattice constants [18]. Our magnetic calculations are spin-polarized (i.e. collinear magnetization) and are employed for any structure containing 50% Fe or higher.

VASP solves for the self-consistent electronic structure in reciprocal space, using a plane wave basis. It is crucial to choose the reciprocal space grid appropriately and demonstrate convergence in the number of k-points used and the plane wave energy cutoff. We choose k-point grids whose spacing is nearly isotropic in reciprocal space. Mostly we use Monkhorst-Pack grids, although for hexagonal structures we use Gamma-centered grids. Our k-point density is sufficient that all structural energies are converged to a precision of 10 meV/atom or better. All energies for structures that lie on or near the convex hull are converged to a precision of 1 meV/atom or better.

In general our relaxations allow variations of cell volume and shape, as well as atomic displacements, consistent with the symmetry of the starting structure. Relaxations run until an accuracy of 1meV/atom or better is reached. During relaxation we use Methfessel-Paxton Fermi-surface smearing with width 0.2 eV (the VASP default choice [19]. When smearing is employed we report the *energy* (extrapolated to zero smearing), not the fictitious *free energy*. For structures on or near the convex hull, we recalculate the energy of our best-relaxed structure using the tetrahedron method without smearing.

Convergence with respect to k-point grid and plane wave cutoff energy is demonstrated in table I. We examine here the structures and energies of two metastable variants of Fe_3B, one with structure type Fe_3C.oP16 and one with structure type Ni_3P.tI32. From the data in table I we see how energies E and energy differences ΔE converge as the k-point mesh grows at fixed energy cutoff. However, the energy difference ΔE at low precision has even the incorrect sign, while medium and high precision agree to within the desired 1meV/atom accuracy.

Certain calculated structural quantities can be compared directly with experiment. For example, for Fe_3B.oP16 we obtain converged volume 9.78 $Å^3$/atom, $b/a = 1.23$ and $c/a = 1.52$ compared with the experimental values, respectively, of 10.09 $Å^3$/atom, 1.22 and 1.51. Likewise, for Fe_3B.tI32 we find volume 9.61 $Å^3$/atom and $c/a = 2.03$ compared with experimental values 10.06 $Å^3$/atom and 2.01. Our underestimation of the volume reflects both thermal expansion (experimental volumes are room temperature, while our calculations are ground state (i.e. T=0K)) and a known systematic error associated with density functional theory.

The composition space of an N-component alloy is a set of N composition variables $\{x_i, i = 1, 2, ..., N\}$ obeying $\sum_{i=1}^{N} x_i = 1$. The set forms an $N-1$ dimensional simplex (respectively, a point, line segment, triangle and tetrahedron for $N = 1, 2, 3, 4$). The structural energies form a scatter-plot over this simplex. According to principles of thermodynamics, stable low temperature phases lie on vertices of the convex hull of the energy versus composition scatter-plot. Edges and facets of the convex hull represent coexistence regions of the phases that lie at adjoining vertices. An alloy whose composition is on a convex hull edge or facet will decompose into a mixture of the phases at the vertices. Lines and triangles joining low temperature phases phases will be refered to as tie-lines and tie-planes. A tie-surface in general refers to the hyperplane joining N or fewer points in the N-component energy scatter-plot.

The tie-surface connecting all pure elements in their lowest energy structures forms a useful reference for alloy energies. The distance ΔH_{for} of an alloy energy from the tie-surface joining pure elements is known as its enthalpy of formation (enthalpy because our volume relaxation

TABLE I: Converence of magnetization and energy with respect to k-point density and plane wave cutoff. Numbers in left-hand column are the product of lattice parameter times the number of k-point subdivisions. Values of E_c are plane wave cutoff energies in eV

Param		Fe3C.oP16		Ni_3P.tI32		
grid	E_c	M	E	M	E	Δ_E
1	239	1.38	-8.1227	0.37	-8.1073	0.0155
10	239	1.16	-7.9698	0.80	-7.9283	0.0415
20	239	1.29	-8.0460	1.33	-8.0519	-0.0059
28	239	1.22	-7.9870	1.27	-7.9899	-0.0029
36	239	1.20	-7.9629	1.26	-7.9656	-0.0027
44	239	1.20	-7.9554	1.26	-7.9572	-0.0017
52	239	1.20	-7.9525	1.25	-7.9543	-0.0018
1	319	1.38	-8.1725	0.82	-8.0873	0.0852
10	319	1.51	-8.0683	1.33	-8.0365	0.0318
20	319	1.49	-8.0430	1.38	-8.0428	0.0002
28	319	1.48	-8.0441	1.39	-8.0420	0.0020
36	319	1.49	-8.0437	1.39	-8.0409	0.0028
44	319	1.50	-8.0437	1.39	-8.0410	0.0027
52	319	1.50	-8.0437	1.39	-8.0411	0.0026
1	398	1.38	-9.1688	1.43	-8.0991	0.0696
10	398	1.50	-8.0667	1.51	-8.0667	0.0334
20	398	1.48	-8.0382	1.38	-8.0383	-0.0001
28	398	1.48	-8.0390	1.39	-8.0372	0.0018
36	398	1.48	-8.0386	1.38	-8.0362	0.0025
44	398	1.49	-8.0386	1.39	-8.0362	0.0024
52	398	1.49	-8.0386	1.39	-8.0363	0.0023

means we work at fixed pressure, $P = 0$). Strong compound formation is reflected in large negative enthalpy of formation.

High temperature phases should lie above the convex hull, but sufficiently be close that entropic effects (e.g. phonons or chemical substitution) can stabilize them. Metastable phases also should lie close to the convex hull, so that their free energy is less than the liquid free energy at temperatures below freezing. Although ΔH_{for} is usually negative for high temperature and metastable phases, their energy difference ΔE from the convex hull is small and positive. The value of $\Delta E > 0$ is a measure of the thermodynamic driving force for the transformation to the appropriate combination of stable phases.

We also define $\Delta E < 0$ for stable phases as the energy difference between the stable structure and the composition-weighted average energy of phases connected to it by edges of the convex hull. This gives a measure of the thermodynamic driving force favoring the given structure over a combination of competing nearby structures.

Using the *ab-initio* methods described above, we built a database of structural energies. For a given N-component alloy system of interest we extract from our database energies of structures containing all, of just some, of the chosen elements. We use a standard convex hull program (qhull [20]) to identify stable structures and the coexistence regions that connect them. Based on the output of this program, we calculate values of ΔH_{for} and ΔE for every structure.

Our methods introduce systematic errors assoicated with the PAW implementation and even with the underlying density functional theory. Provided that the errors vary smoothly with composition, the identity of convex hull vertices will not be affected in most cases. However, the tie-lines, tie-planes, etc. grow progressively more sensitive to error. It is probable that even when we correctly identify the stable phases, we may misidentify their coexistence regions.

Previous workers have carried out analagous studies, though mainly on binary alloys. Hafner [21] wrote a general introduction to the subject of *ab-inito* alloy phase diagram prediction. Miedema, de Boer and coworkers [22] have carried out extensive semi-empirical analysis of binary alloy systems, including almost all binary alloys of Fe [23]. Others [24–26] take more rigorous approaches, sometimes including finite temperature effects of vibrational and configurational entropy.

III. RESULTS

The $N = 4$-component B-Fe-Y-Zr quatenary alloy system contains many subsystems: four pure elements, six binary alloy systems and four ternaries. This section presents our results in order of increasing number of components. We adopt alphabetical order in naming alloy systems, because this brings some order to the proliferation of chemical combinations in multicomponent systems.

As will be seen, in most cases we reproduce the known equilibrium and metastable phase diagrams with surprising accuracy. In some cases where the existence of a phase was known experimentally but not its structure we can offer a suggestion of a probable structure. In a few cases there are lingering discrepancies, some of which may be limitations of our method and others cast doubt on the accepted phase diagrams. Our quatenary and two of our ternary phase diagrams have never been determined experimentally.

A. Pure elements

Each of the four elements under study exhibits solid-solid phase transitions in addition to its melting transition, and verifying the relative energies of the different structures is a nontrivial test of our calculational method.

The precise low temperature structure of Boron is unknown. The equilibrium phase, designated β is rhombohedral with about 108 atoms per unit cell (B.hR108). The atomic positions are known, but there is partial occupancy and probably strong correlations among the partially occupied sites, that have not been adequately resolved. We attempted to optimize the partial occupancy using a "fixed site" Monte Carlo method to eliminate short bonds, but it seems that other constraints must be met in addition. for our present study we use the metastable α structure (B.hR12) in lieu of the true ground state. Indeed, our calculations find $E_\beta - E_\alpha > 0$, while it should be negative, confirming that our structure for β is not adequate.

Pure elemental Iron passes through four solid phases, α-δ, as temperature rises from T=0K to melting. α is BCC (Pearson cI2) and ferromagnetic. At its Curie temperature it transforms to β which is also BCC. At higher temepratures it transforms to γ, which is FCC (Pearson cF4) which is nonmagnetic and finally to δ, again BCC, before melting. Our calculations support the preference for BCC, but the energy difference $E_{FCC} - E_{BCC}$=119 meV/atom is probably too high because we do not account for local magnetic moment formation in the FCC structure. First-principles calculations [27] show that the magnetic ground state of γ-Fe is a noncollinear antiferromagnet, while at the experimental atomic volume it is a collinear antiferromagnet [28]. According to our calculations, the relaxed energy of this antiferromagnetic structure is 81 meV/atom above the energy of α-Fe.

The low temperature α phases of Yttrium and Zirconium are both hexagonal (hP2) and their high temperature β phases are both BCC (cI2). Our calculations agree with these facts.

B. Binaries

1. Fe-B

The established Fe-B phase diagram contains just two compounds, Fe_2B.tI12 and BFe.oP8, each with simple structures. A number of metastable phases exist in the Fe-rich end, namely Fe_3C.oP16, Ni_3P.tI32 and C_6Cr_{23}.cF116. These occur close to the deep eutectic at 17 % B, and hence are important competitors to glass formation.

Our calculations shown in Fig. 1 (top left) reproduce the established phase diagram perfectly, with the known stable phases lying on the convex hull and the known metastable phases lying within 20 meV/atom above. Note that at the eutectic melting temperature of T=1447 K, a characteristic thermal energy is $k_B T = 125$ meV/atom. Other structures that occur as stable or metastable phases in similar metal-metalloid systems (but not in Fe-B) lie further above the convex hull, except for the BRe_3.oC16 structure. On the basis of our calculation BRe_3 *should* occur as a metastable phase in Fe-B, although to our knowledge it has not been reported.

A prior *ab-initio* study of the Fe-B structures investigated magnetism and bonding [29]. That study reported a covalent character to Fe-B and B-B bonds while the Fe-Fe bonds are metallic in nature, together with a significant charge transfer from Fe to B. Spin polarization of the B atoms is weak and *opposite* to the Fe atoms. Our calcuations support those conclusions.

Given our perfect agreement with the establishhed phase diagram, it is suprising that our calculated enthalpies (respectively -368 and -308 meV/atom for FeB and Fe_2B) differ greatly from measured values (respectively -676 and -707 meV/atom for FeB and Fe_2B [30]). This is probably due in part to the fact that our calculation are performed at T=0K while the measurements were done at T=1385K. Pure elemental Fe undergoes two phase transitions (one structural, one magnetic) as temperature drops, which surely is at least partly responsible for this discrepancy.

One hypothesis on the glass-forming ability of Fe-B is that very simple, easy to nucleate and grow crystal structures, are destabilized by the size contrast [31] of Fe (nominal diameter=2.48Å) and B (nominal diameter=1.80Å). We can observe this principle in action in the Fe-rich end of this phase diagram. Consider a substitutional solid solution of Fe and B, around composition Fe_3B, based on the BCC structure of Fe. The Fe_3Si.cF16 structure is a particular realization of such a structure, in which the Fe and B atoms arrange at regular positions. However, the energy of cF16 is much higher than the metastable oP16 structure, which can be reached through strong distortions of the cF16 lattice. It seems that the lattice strain caused by size mismatch destabilizes the BCC solid solution, converting cF16 into oP16.

We note in addition that B will not stabilize the FCC structure of Fe by substitution to form the AuCu3.cP4 structure.

Alternatively, B might enter as an interstitial, as indeed C enters into FCC lattices of Fe in octahedral or tetrahedral sites (respectively, in the metastable Fe_3C.hP8 and Fe_4C.cP5 structures). However, owing to the slightly larger size of B compared with C (nominal diameter=1.43Å), these structures are far above the convex hull in the B-Fe energy scatter plot.

It seems that only fairly complicated crystal structures exist near compositions of about 25 % B. The difficulty of nucleating and growing these structures may aid in glass formability. An estimate of the thermodynamic driving force for nucleation can be obtained by comparison of three energy scales. The metastable structures are about 10-20 meV/atom above the tie-line joining Fe_2B to α-Fe. A quenched amorphous structure at composition $Fe_{80}B_{20}$ is about 170 meV/atom above the tie-line, and the liquid is 350 meV/atom above. Our procedure for calculating amorphous and liquid energies is described in section IV B.

2. Fe-Zr and Fe-Y binaries

A promising glass-forming strategy is to start with a good glass-forming binary such as B-Fe, then add one or more additional elements to further destabilize any crystalline structures. Large atoms such as Zr (nominal diameter=3.18Å) and Y (nominal diameter=3.55Å) are promising because they associate well with Fe and B but they differ strongly in size from either Fe or B. Before

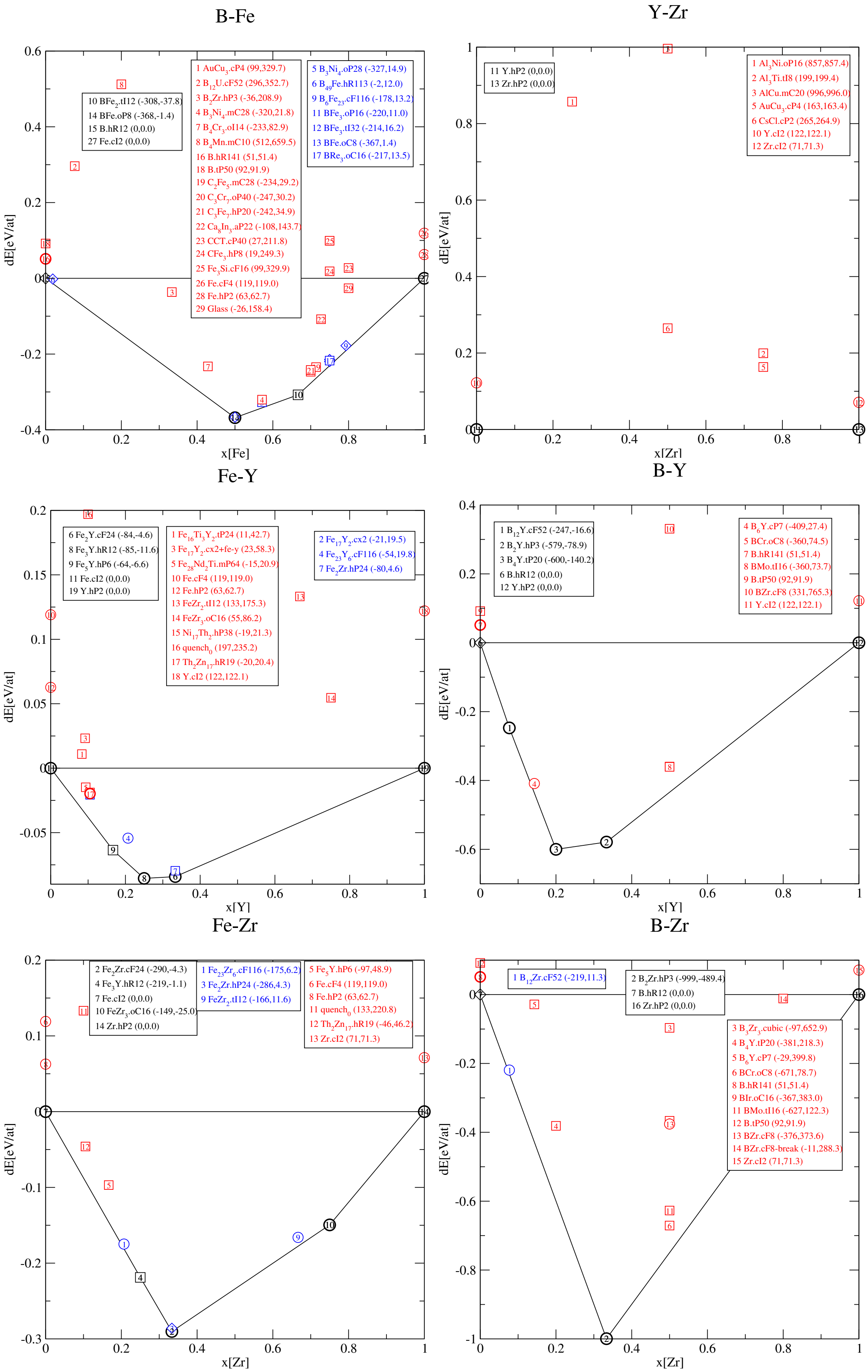

FIG. 1: Enthalpies of formation and their convex hulls for all binaries in the B-Fe-Y-Zr system. Notation: heavy circles denote known low temperature phases, light circles denote known high temperature phases, diamonds denote known metastable phases, squares denote unreported structures.

turning to these ternary compounds, we briefly examine the Fe-Zr and Fe-Y binaries.

The established Fe-Zr phase diagram [32] contains three low temperature compounds, Fe_2Zr.cF24, $FeZr_2$.tI12 and $FeZr_3$.oC16, one high temperature compound $Fe_{23}Zr_6$.cF116 (this cF116 structure is quite distinct from the C_6Cr_{23}.cF116 structure which confusingly shares the same stoichiometry and Pearson symbol) and one metastable compound Fe_2Zr.hP24.

Again, our calculations (see Fig. 1) are in excellent agreement with experiment. Every known low temperature phase lies on the convex hull, and the high temperature and metastable compounds lie close above it.

One unknown structure, Fe_3Y.hR12, appears on the convex hull where no stable compound is known experimentally. Most likely this reflects an inaccuracy of our methods. Because its stability relative to the tie-line joining Fe_2Zr to pure Fe is only ΔE=-1.1 meV/atom, small errors (either calculational or arising from approximations of density functional theory) could account for this difference. Alternatively, the phase could truly be stable, but hard to observe experimentally because its small ΔE means the driving force for its formation is weak. This matter requires further theoretical and experimental analysis, but for the study of glass formation all we care about is that its energy lies close to the tie-line from Fe_2Zr to α-Fe.

Now consider Fe-Y. The established phase diagram [32] contains all the same phases as Fe-Zr and two additional phases, Fe_3Y.hR12 and $Fe_{17}Y_2$. Certain features of the phase diagram are thermodynamically improbable [33]. Of particular note, the close proximity of line compound $Fe_{23}Y_6$.cF116 (at low temperature) to the line compound Fe_3Y.hR12 is highly unlikely. We presume that $Fe_{23}Y_6$.cF116 is stable at high temperatures only, where the phase diagram shows a broad composition range. The strong asymmetry of the liquidus of Fe_3Y.hR12 also is improbable but we have no proposed alternative at present.

The structure of $Fe_{17}Y_2$ has not been properly identified, and is believed to occur in at least two variants. We will follow the lead of Massalski and Okhamoto and identify these variants as Th_2Zn_{17}.hR19 (low temperature) and $Ni_{17}Th_2$.hP38 (high temperature). Other reported variants [9] of this phase are $Fe_{17}Ho_2$.hP44 and $Ni_{19}Th_2$.hP80. The occurrence of several structural variants, most with partial occupancy, suggest a possible entropic stabilization mechanism by structural disorder. There is a synopsis of the basic structure and its degrees of freedom in the discussion section IV.

Our calculations for Fe-Y (Fig. 1) present certain disagreements in comparison with experiment. Notably, the $Fe_{23}Y_6$.cF116 structure and all variants of $Fe_{17}Y_2$ lie above the convex hull and thus are predicted as high temperature or metastable. Meanwhile, Fe_5Y.hP6, believed metastable touches the convex hull with a value ΔE=-6.6 meV/atom that is probably significant. As discussed already, it seems very likely that $Fe_{23}Y_6$ is only a high temperature phase, as it is in Fe-Zr. Perhaps the broad composition range stabilizes the structure by means of configurational entropy.

For the appearance of Fe_5Y instead of $Fe_{17}Y_2$, three possible explanations are: (1) The structure of $Fe_{17}Y_2$ has not yet been correctly determined; (2) Our calculations are seriously flawed and unable to properly compare the energies of Fe-Y compounds; (3) $Fe_{17}Y_2$ is only metastable or high temperature and the true low temperature phase is Fe_5Y. Concerning (1), we previously mentioned that the $Fe_{17}Y_2$ structure has not been fully determined. Concerning (2) we explored refinements of the calculation such as inclusion of spin-orbit coupling, use of other pseudopotentials and change in the cutoff energy, but none of these efforts resolved the problem.

The most likely explanation for the energy of $Fe_{17}Y_2$ lying above the convex hull (in our view) is that this phase is actually a *high temperature* equilibrium phase only. A simple mechanism to explain high temperature stability is note that the energy of $Fe_{17}Y_2$ lies *below* the tie-line from Fe_5Y to γ-Fe. Because γ-Fe is the phase with which $Fe_{17}Y_2$ coexists from melting down to about T=900C, it may be difficult to observe decomposition of $Fe_{17}Y_2$ at low temperatures where it competes instead with α-Fe. This scenario suggests the possibility that other Fe-based alloy phase diagrams could be incorrect at low temperatures, which could have significance for the engineering of magnetic materials [6].

The *ab-initio* calculations of total energies for the Fe-Zr and Fe-Y alloys were difficult because of the complicated magnetic properties of the Fe-rich structures. We mention two important observations. (1) The Zr and Y atoms have magnetic moments pointing opposite to the Fe atoms. Moments are typically in the range of +1.8 to +2.4 μ_B for Fe and in the range of -0.2 to -0.4 μ_B for Y or Zr in spin polarized calculations. Similar values for Fe-Y alloys were reported in prior calculations [34] and experiments [35]. (2) Magnetism couples strongly with atomic volume leading to multiple self-consistent solutions of the DFT. Generally one finds: a nonmagnetic, low volume, high energy solution; a strongly magnetic, high volume, low energy solution; occasional additional solutions of intermediate magnetism, volume and energy. Presumably this is related to the strong magnetovolume effects that actually occur in Fe-rich compounds [6, 34].

Comparing our calculated enthalpies of formation with published experimental data [30], we again find that our calculated values lie well below the published data, in the case of Fe-rich alloys, probably as a result of the high temperatures at which the experiments were carried out. At lower Fe-content our data is fairly consistent with the experimental data.

3. Other binaries: B-Zr, B-Y and Zr-Y

Next we turn to the B-Zr and B-Y binaries. The established B-Zr phase diagram exhibits three compounds. The well known stable phase ZrB2.hP3 is very strongly bound (we find enthalpy of mixing of nearly 1/2 eV/atom). The other two phases exist only at high temperatures. ZrB12.cF52 melts congruently, while ZrB.cF8 exists only over an intermediate temperature range below all liquidus temperatures [36, 37]. Our calculation (Fig. 1) supports stability of ZrB2 and high temperature stability of ZrB12, but strongly contradicts the existence of BZr.cF8. Indeed, at this composition the best structure we find is BCr.oC8, but that too is highly unstable. We have explored nearby compositions, and even added traces of C (ZrC.cF8 *is* a stable compound in the C-Zr binary system), but we cannot find any structure within a reasonable distance of the convex hull. Our conclusion is that ZrB.cF8 is probably a metastable structure formed during rapid quench [36, 37].

Comparing our calculated enthalpies of formation with published data [30] we find excellent agreement. For $B_{12}Y$ we calculate -219 meV/atom compared with the experimental value -213 meV/atom. The experimental data is taken at a fairly low T=298K. For B_2Zr we calculate ΔH_{for}=-999 meV/atom compared with the experimental value -1074 meV/atom.

The enthalpy of B_2Zr is very negative as a result of strong covalent B-B bonding. Densities of states among transition-metal diboride[38] exhibit a strong pseudogap associated with Boron p-states. As one moves across the transition-metal series, the Fermi level falls in the pseudogap for group IVa elements (Ti/Zr,Hf), leading to strong peaks in cohesive energy. This is also the likely cause of the wide composition range of B_2Nb - since Nb lies just to the right of Zr and the Fermi energy of B_2Nb lies just to the right of the pseudogap, Nb vacancies can move the Fermi energy closer to the gap, resulting in a low vacancy formation energy.

In contrast to B-Zr, B-Y contains several B-rich phases, including B2Y.hP3 and B12Y.cF52 as in B-Zr, and additionally B4Y.tP20 and B6Y.cP7. The last one is of uncertain composition [10]. Finally, there is a phase B66Y.cF1880 of gigantic unit cell size, which is too large for us to calculate. Our calculated convex hull (Fig. 1) agrees perfectly with this experimental data. In the case of B_6Y it was necessary to construct a $2 \times 2 \times 2$ supercell and remove a Y atom to reach the convex hull. No experimental data is available for enthalpy of formation.

Finally, consider the Zr-Y binary. The established phase diagram contains no compounds. We investigated several possibilities appropriate for their atomic size ratio and found none stable.

C. Ternaries

1. *B-Fe-Zr and B-Fe-Y*

The ternary alloy system B-Fe-Zr exhibits no known ternary compounds. Our calculations (Fig. 2) generally support this, but we do identify one structure, B_4CrY.oP24, which lies 52 meV/atom below its tie-plane, and hence is predicted to be stable. Interestingly, we identify this structure as a decagonal quasicrystal approximant. No B-based quasicrystals are currently known. We convert the binary structure C_6Cr_{23}.cF116 to a ternary by substituting the large Zr atoms on the which have the largest Voronoi volume. These turn out to sites of Wyckoff type $8c$, resulting in the intrinsic ternary structure type B_3Fe_{13}Nb.cF116. Interest in this structure is motivated by its proximity to the glass-forming composition, and the metastability of this structure is discussed later, in section IV. The quenched structure is, as before, a model metallic glass.

The reason that B-Fe-Zr exhibits so few (i.e. just one) stable ternary compounds is that the enthalpy of formation of B_2Zr is very large, as discussed above in section III B 3. The covalent bonding of B_2Zr is so strong that even Fe-rich systems find it advantageous to phase separate into a mixture of B_2Zr plus Fe alloyed with which ever of Zr or B remains in excess.

In contrast, the B-Fe-Y ternary alloy system exhibits many stable ternary compounds, because the bonding of B_2Y is less strong than B_2Zr. Those compounds with known structures are the Fe-rich compound BFe14Y2.tP68, and in the Fe-poor region B2Fe2Y.tI10, B6Fe3Y4.hR13, B7FeY3.oC44 and a metastable structure B14Fe62Y3.cI158. Additionally there are stable compounds of unknown or partially known structure at B3FeY2, B4Fe4Y and B4FeY. Our calculations reveal these compounds to take the structure types, respectively, B6Fe2Nd5.hR13, B4Co4Nd.tP18 and B4CrY.oP24.

All previously known structures are also on the convex hull. Surprisingly, we find a previously unknown compound of structure type BCeCo4.hP12 on the convex hull in the Fe-rich region. Nearby we find structure type $B_2Nd_3Ni_{13}$.hP18 is nearly on the convex hull. It would be of considerable interest to explore these compositions experimentally in more detail.

One structure reported in the B-Fe-Y system, B14Fe62Y3.cI158, has a very high energy (ΔE = 330 meV/atom) and large initial forces (as high as 1.7 eV/Å). Even after large atomic displacements during relaxation the energy remains very high. We believe the solved structure is incorrect.

We are impressed by the faithfulness with which our calculations reproduce systematic differences in the phase diagrams of Y- and Zr-containing alloys. Despite their adjacency in the periodic table, and the consequent similarities in atomic size, electronegativity and prefered structure types, those details on which the accepted phase diagrams *do* differ are almost always correctly reproduced.

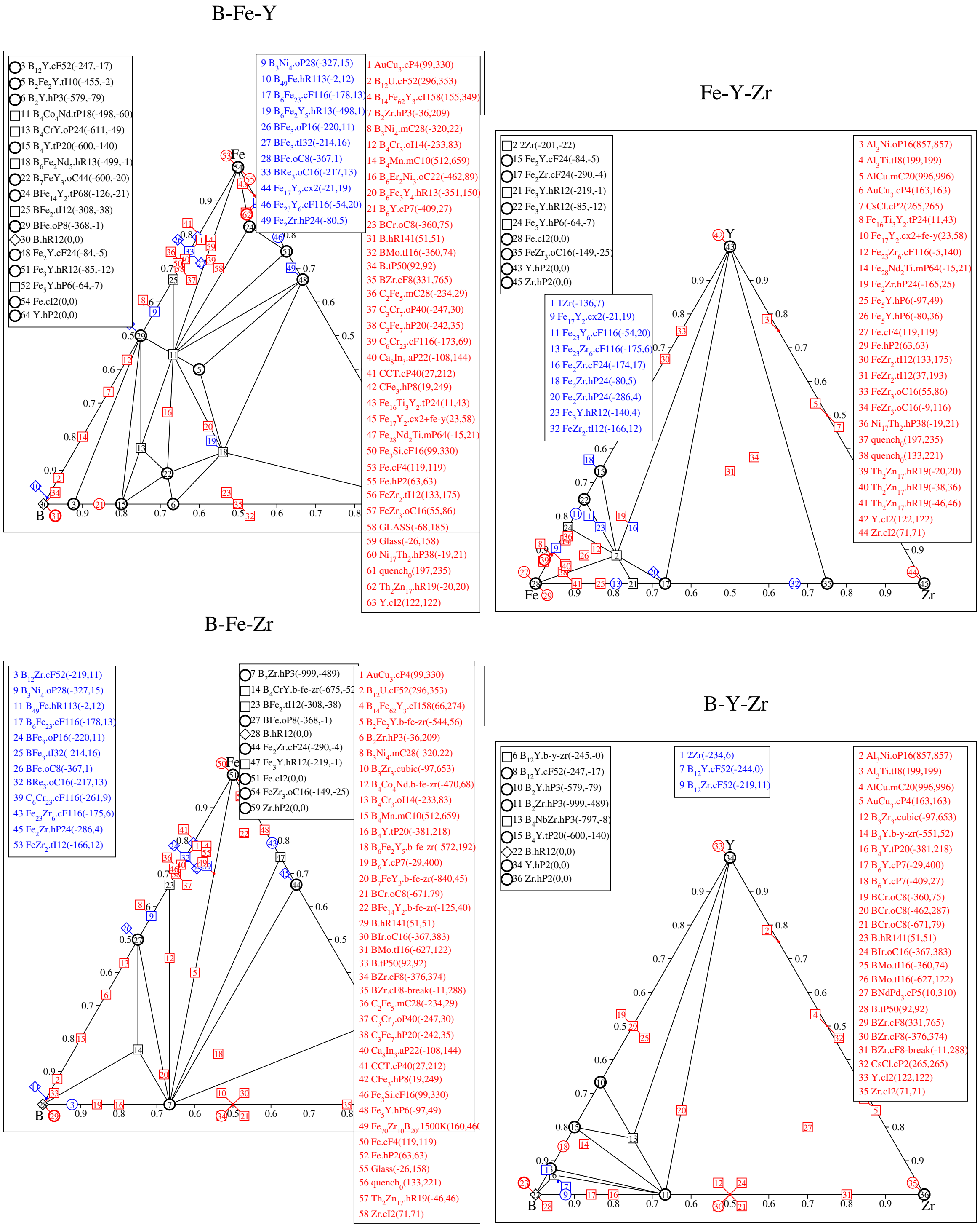

FIG. 2: Convex hulls of ternaries in the B-Fe-Y-Zr system. Plotting symbols as in Fig. 1.

2. B-Y-Zr and Fe-Y-Zr

The B-Y-Zr ternary diagram has not been experimentally determined. We have explored it using the methods described above. The only stable ternary compounds we find are extensions of certain binaries into the ternary. Notably (Zr,Y)B2.hP3 exhibits complete miscibility of Zr and Y in this pseudobinary structure. Additionally, B_{12}Y.cF52 extends part way into the ternary.

The Fe-Y-Zr ternary diagram has not been experimentally determined either. Our calculations suggest that Fe_2(Y,Zr).cF24 and Fe_3(Y,Zr).hR12 both extend across the full ternary diagram, but no other binaries appear to extend far into the ternary.

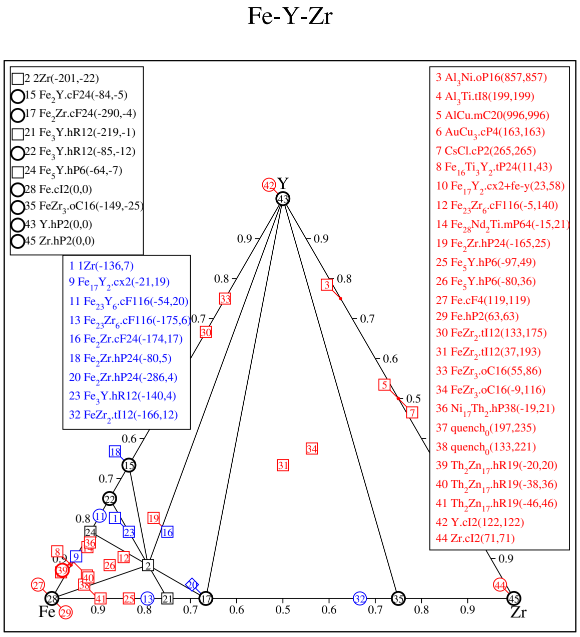

FIG. 3: Convex hull of quatenary system B-Fe-Y-Zr. Diagram is contained in a tetrahedron with pure elements at vertices. This is a view along the axis from pure B to the center of te Fe-Y-Zr triangle. Plotting symbols as in Fig. 1.

D. B-Fe-Y-Zr Quaternary

The B-Fe-Y-Zr quatenary has not been experimentally determined. No quatenary structures are reported in the standard references. We have calculated enthalpies of formation for 15 different compounds (11 structure types, some with alternate chemical occupancies) and find no stable quatenaries (see Fig. 3). The nearest we come to stability is for the structure type B_4CrY.oP24, for which ΔH_{for} is around 3-4 meV/atom for all substitutions of Y and Zr. Thus it is likely that the entire Y/Zr substitution yields equilibrium structures at high temperatures. We find 4 meV/atom for substitution of Zr for one of the two Y in $BFe_{14}Y_2$.tP68, suggesting significant Zr solubility at high temperatures.

IV. DISCUSSION

THIS SECTION TO BE WRITTEN BY MIKE&MAREK.

DISCUSSION OF ATOMIC MOTIFS IN STRUCTURES, PACKING DENSITY, ETC.

STRUCTURE OF FE17Y2 INCLUDING CONFIGURATIONAL DEGREES OF FREEDOM AND AN ASSESSMENT OF CONFIGURATIONAL ENTROPY. Note stacking disorder model (experimental) [35] similar to random stacking of sheets of Fe-dumbels and Y atoms (model) [39].

TABLE II: Enthalpies of crystal phases competing with glass formation.

	Fe3B.oP16	C6Cr23.cF116	BFe14Nd2.tP68
B-Fe	-220	-178	
B-Fe-Y		-178	-126
B-Fe-Zr		-261	-125
	BCr.oC8	AlB2.hP3	NaCl.cF8
B-Y	-360	-579	+331
B-Zr	-671	-999	-376

A. Glass formation

By inspection of the data in Figs. 1 and 2 we can identify the main crystal phases that are likely to compete with formation of the amorphous solid. In the vicinity of Fe80B20, the structure C6Cr23.cF116 can crystalize with almost no composition shift. However, it may be difficult to nucleate and grow such a complex crystal type during a quench, so a simpler nearby structure such as Fe_3B.oP16 may be favored. In the limit of slow cooling, phase separation into pure Fe and Fe2B will occur. In fact, all these are reported in annealed samples of Fe-B glasses.

Alloying with Zr can be advantageous because the large and strongly interacting Zr atoms diffuse slowly [40]. Due to its large size, Zr strongly destabilizes the Fe3B.oP16 structure. NEED TO VERIFY THIS. However, we see in table II that Zr actually tends to stabilize slightly the C6Cr23 structure, and also risks formation of the BFe14Nd2.tP68 structure. Stabilization of the C6Cr23 structure may be counteracted with replacement of Y for Zr. Another danger of alloying with Zr is formation of the highly stable binary ZrB2.hP3. Indeed, in the B-Fe-Zr ternary [11] even Fe-rich liquids coexist with solid ZrB2. Again, alloying with the less strongly interacting (but stillvery large) element Y can counteract this.

The reasons to avoid use only Y as opposed to Zr are: 1) Y atoms diffuse more quickly than Zr as a result of their weaker binding. 2) There are several Fe-rich Fe-Y binary structures (e.g. Fe5Y, Fe17Y2) whose formation should be avoided.

Recent experimental studies [41, 42] of Y addition to Fe-Zr-B-based glasses confirm its beneficial effects, while attributing them to different causes [41].

B. Liquid and Amorphous Structures

Candidate liquid and amorphous structures were produced following the procedure outlined in reference [40]. Briefly, we performed liquid state molecular dynamics on 100 atom samples using Nosé dynamics at temperature T=1500K. Three liquid samples were taken, at 200 fs intervals, and quenched by conjugate gradient relaxation in the manner described above. Atomic displacements under relaxation are large, averaging about 0.6 Å. The liquid runs were at fixed volume, 7% greater than the volume of the quenched amorphous samples. All molecular dynamics and relaxation runs were done with spin polarization, using the Γ k-point only.

C. Amorphous Approximants

THIS SECTION TO BE WRITTEN BY MAREK.

V. CONCLUSIONS

In conclusion, we present a method for the calculation of low temperature (T=0K) alloy phase diagrams and apply it to the study of the B-Fe-Y-Zr quatenary system. A key distinguishing feature of our approach is the establishment of two databases: one from which we draw promising structures oserved in similar chemical systems; the other in which we record our calculated cohesive energies which can be quickly converted into enthalpies of formation. The first database allows us to propose and evaluate candidate structures even in alloy systems that have not been previously studied. The second allows us to quickly add a new chemical element, and re-use, for example, all our B-Fe-Zr data in the study of the B-Fe-Y-Zr quatenary.

As a result we have examined two new ternary systems (B-Y-Zr and Fe-Y-Zr) and the B-Fe-Y-Zr quatenary. We found certain binary phases extending into the new ternary systems, and certain ternary phases extending into the quatenary. So far we have not discovered a stable quatenary structure, not related to an adjoining ternary. Perhaps none exists, although it is possible that we simply have not tried the right one.

Strong disagreements between calculated and reported phase diagrams come in 3 types.

1. Uncertain reported structure found to have high energy (e.g. BZr.cF8). Likely cause is the structure is actually metastable or else reported structure is in error.

2. Structure calculated to be stable not present in published diagram. Further experimental study of this composition range may be warranted. (e.g. B_4CoZr in B-Fe-Zr).

3. Well established experimental structure (e.g. $Fe_{17}Y_2$) found to have high energy. Likely causes are disorder or partial occupancy requiring further theoretical study. Other effects such as noncollinear magnetism should also be investigated.

Weak disagreements occur when presumed low temperature structures lie slightly above the convex hull in our calculation (e.g. ?) or unreported structure touches convex hull with small ΔE (e.g. Fe5Y in Fe-Zr system). These cases want both experimental and theoretical study. It is not clear which is more reliable.

Comparison of our calculated enthalpies with experimental data revealed systematic disagreements with Fe-rich enthalpies lying way below experimental values. An obvious source of disagreement is that the experimental enthalpies are measured at high temperatures, and magnetic and structural phase transitions prevent a simple extrapolation to low temperatures. However, we do not claim that our calculated enthalpies are quantitatively accurate. Systematic errors introduced by density functional theory may interfere. As long as these errors vary smoothly with composition, however, the convex hull vertices will rarely be affected.

Acknowledgments

We wish to acknowledge useful discussions with Yang Wang, Don Nicholson, Joe Poon and Gary Shifflet. This work was supported by DARPA/ONR Grant N00014-01-1-0961.

[1] G. Olson, Science **288**, 993 (2000).
[2] T. Z. A. Inoue and T. Masumoto, Mat. Trans. JIM **31**, 177 (1990).
[3] A. Peker and W. Johnson, Appl. Phys. Lett. **63**, 2342 (1993).
[4] R. S. Y. He and J. Archuleta, Appl. Phys. Lett. **69**, 1861 (1996).
[5] W. Johnson, MRS Bulletin **24**, 54 (1999).
[6] J. Coey, ed., *Rare-Earth Iron Permanent Magnets* (Oxford, Oxford, 1996).
[7] G. Kresse and J. Hafner, Phys. Rev. B **47**, RC558 (1993), Kresse and Furthmuller [8].
[8] G. Kresse and J. Furthmuller, Phys. Rev. B **54**, 11169 (1996).
[9] P. Villars, *Pearson's Handbook, Desk Edition* (ASM International, Materials Park, Ohio, 1997).
[10] e. a. T.B. Massalski, ed., *Binary Alloy Phase Diagrams* (ASM International, Materials Park, Ohio, 1990).
[11] A. P. P. Villars and H. Okamoto, *Handbook of ternary alloy phase diagrams* (ASM International, Materials Park, Ohio, 1995).
[12] P. Gaskell, Nature **276**, 484 (1978).
[13] V. Elser and C. Henley, Phys. Rev. Lett. **55**, 2883 (1985).
[14] Y. Wang and J. Perdew, Phys. Rev. B **44**, 13298 (1991).
[15] G. Kresse and D. Joubert, Phys. Rev. B **59**, 1758 (1999).
[16] J. Perdew and Y. Wang, Phys. Rev. B **45**, 13244 (1992).
[17] L. W. S.H. Vosko and M. Nussair, Can. J. Phys. **58**, 1200 (1980).
[18] J. H. E.G. Moroni, G. Kresse and J. Furthmuller, Phys. Rev. B **56**, 15629 (1997).
[19] G. Kresse and J. Furthmuller, http://cms.mpi.univie.ac.at/vasp (2003).
[20] D. D. C.B. Barber and H. Huhdanpaa, ACM Trans. Math. Software **22**, 469 (1996).

[21] J. Hafner, *From Hamiltonians to Phase Diagrams* (Springer-Verlag, Berlin, 1987).
[22] *et al.*. F.R. de Boer, *Cohesion in metals:transition metal alloys* (North-Holland, Amsterdam, 1988).
[23] A. N. R. Boom, F.R. de Boer and A. Miedema, Physica **115B**, 285 (1983).
[24] M. A. , *et al.*, Phys. Rev. B **59**, 14271 (1999).
[25] M. Sluiter and Y. Kawazoe, Europhys. Lett. **57**, 562 (2002).
[26] C. W. V. Ozolins and Z. Zunger, Phys. Rev. B **58**, R5897 (1998).
[27] E. Sjostedt and L. Nordstrom, Phys. Rev. B **66**, 014447 (2002).
[28] E. H. H.C. Herper and P. Entel, Phys. Rev. B **60**, 3839 (1999).
[29] W. C. *et al.*, Phys. Rev. B **42**, 4460 (1990).
[30] O. Madelung, ed., *Landolt and Bornstein, New Series, Group IV*, vol. 5 (Springer-Verlag, Berlin, 1992).
[31] T. Egami and Y. Waseda, J. Noncryst. Solids **64**, 113 (1984).
[32] H. Okamoto, ed., *Desk Handbook: Phase Diagrams for Binary Alloys* (ASM International, Materials Park, Ohio, 2000).
[33] H. Okamoto and T. Massalski, chapter in [32] (2000).
[34] R. Coehorn, Phys. Rev. B **39**, 13072 (1989).
[35] e. a. O. Moze, Phys. Rev. B **50**, 9293 (1994).
[36] F. Glaser and B. Post, Trans. AIME **197**, 1117 (1953).
[37] Y. Champion and S. Hagege, J. Mat. Sci. Lett. **11**, 290 (1992).
[38] C. R. P. Vajeeston, P. Ravindran and R. Asokamani, Phys. Rev. B **73**, 045115 (2001).
[39] e. a. W. Coene, J. less-common metals **157**, 255 (1990).
[40] *et al.*. M. Widom, MRS Conf. Proc. **??**, ??? (2002).
[41] C. L. Z.P. Lu and W. Porter, Appl. Phys. Lett. **83**, 2581 (2003).
[42] S. Poon, Unpublished (2003).